General bounded corner states in the two-dimensional Su-Schrieffer-Heeger model with intracellular next-nearest-neighbor hopping

Xun-Wei Xu [1,*] Yu-Zeng Li,[1] Zheng-Fang Liu,[1] and Ai-Xi Chen[2,1,†]
[1]*Department of Applied Physics, East China Jiaotong University, Nanchang 330013, China*
[2]*Department of Physics, Zhejiang Sci-Tech University, Hangzhou 310018, China*

(Received 8 April 2020; accepted 8 June 2020; published 29 June 2020)

We investigate corner states in a photonic two-dimensional (2D) Su-Schrieffer-Heeger (SSH) model on a square lattice with zero gauge flux. By considering intracelluar next-nearest-neighbor (NNN) hoppings, we discover a broad class of corner states in the 2D SSH model and show that they are robust against certain fabrication disorders. Moreover, these corner states are located around the corners but not at the corner points. We analytically identify that these corner states are induced by the intracelluar NNN hoppings (long-range interactions) and split off from the edge-state bands. Thus, we refer to them as general bounded corner states. Our paper shows a simple way to induce unique corner states by the long-range interactions and offers opportunities for designing novel photonic devices.

DOI: 10.1103/PhysRevA.101.063839

I. INTRODUCTION

Topological photonics is a rapidly emerging research field based on topological band theory [1], inspired by topological phases and phase transitions in solid-state electron systems. It provides us the geometrical and topological ideas to design and control the behavior of photons, leading to interesting phenomena, such as the properties of against backscattering and robust to defects and disorders. To highlight one important example, topologically protected photonic modes have been used both theoretically and experimentally to demonstrate a topological insulator laser in a topological edge state (ES) [2–6]. In recent years, a class of interesting topological phases has been introduced in photonic topological systems, such as topological phases of non-Hermitian systems [7–25], a nonlinear-photonic topological phase [26–32], topological quantum matter in synthetic dimensions [33–40], and higher-order topological insulators (HOTIs) [41–47].

In contrast to conventional (first-order) topological states, higher-order topological (HOT) states two or more dimensions lower than the system are hosted in HOTIs [48–54]. To date, the HOT states (e.g., corner states) have been implemented in many different types of photonic lattices, such as the honeycomb lattice [55–57], the kagome lattice [58–61], and the square lattice [62–70].

In this paper, we will focus on corner states in two-dimensional (2D) Su-Schrieffer-Heeger (SSH) model on a square lattice. It has been demonstrated experimentally that the standard 2D SSH model can not support robust corner states for the zero-energy modes are located in the bulk band [66]. To observe a topologically protected corner state in the photonic 2D SSH model, a synthetic magnetic flux of π per plaquette, i.e., negative coupling, was proposed theoretically [41] and demonstrated experimentally [62–66] in some recent works. Besides, topologically protected corner states also have been observed in the band gap in 2D dielectric photonic crystals on the SSH model [67–70], which can be understood by considering the higher-order couplings, such as the next-nearest-neighbor (NNN) coupling between the dielectric rods which inevitably break the chiral symmetry. However, the effects of NNN coupling on topological phases are still an open question at the moment.

Here, we will investigate how to observe corner states in the 2D SSH model with intracelluar NNN hopping in a tight-binding representation. We note that the effects of NNN coupling on topological phases have been explored in bipartite lattices for reconfigurable topological phases [71] and topological defect states [72]. Nevertheless, we find that intracellular NNN coupling can induced new corner states in the 2D SSH model. Different from the conventional corner states observed before, the intracelluar NNN coupling-induced corner states appear around the corners but not at the corner points. We also note that these corner states are similar to the type-II corner states observed in photonic kagome crystals very recently [73]. However, we show that there is a broad class of corner states splitting from the topological edge-state bands with the increasing of the intracelluar NNN coupling not just two type-II corner states observed in Ref. [73]. Thus, we refer to them as general bounded corner states in this paper. Moreover, the general bounded corner states can be understood intuitively by the separate model fragments of the 2D SSH model. Our paper broadens the concept of corner states and provides new ideas for designing novel photonic devices, e.g., a high-Q photonic nanocavity [68,69].

II. TWO-DIMENSIONAL SSH MODEL

We consider a photonic 2D SSH model with $N \times M$ unit cells as shown in Fig. 1. There are four modes A–D in one unit cell with eigenfrequencies ω_a, ω_b, ω_c, and ω_d, where γ

*davidxu0816@163.com
†aixichen@zstu.edu.cn

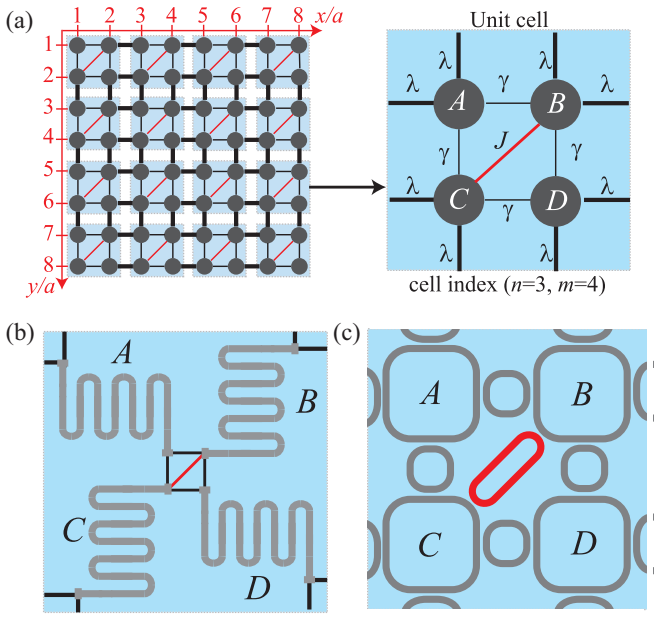

FIG. 1. (a) Schematic of a photonic 2D SSH model on a square lattice. There are four modes (A–D) in one unit cell with lattice constant $2a$, and the amplitudes of intracelluar and intercelluar nearest-neighbor hoppings are γ and λ, respectively. The red oblique lines represent intercelluar NNN hoppings in unit cells with strength J. The possible realistic physical systems to implement one unit cell of the photonic 2D SSH model: (b) network of coupled superconducting transmission line resonators [74–76] and (c) 2D lattice of nanophotonic silicon ring resonators [66].

and λ are the amplitudes of intralar and intercellular (nearest-neighbor) hoppings, and J is the strength of the intracellular NNN hopping (long-range interaction) in unit cells. Different from the model studied in Refs. [62–66], where a synthetic magnetic flux of π per plaquette, i.e., negative coupling, is applied to the square lattices, here, all the hoppings γ, λ, and J are positive, that is, it is a 2D SSH model on a square lattice with zero gauge flux. In the rotating frame with respect to the frequency of all the optical modes $\omega_a = \omega_b = \omega_c = \omega_d = \omega$, the Hamiltonian for the 2D SSH model is described by ($\hbar = 1$)

$$\begin{aligned} H = & \sum_{n=1}^{N}\sum_{m=1}^{M}[\gamma(a_{n,m}+d_{n,m})(b^{\dagger}_{n,m}+c^{\dagger}_{n,m})+Jb_{n,m}c^{\dagger}_{n,m}] \\ & +\sum_{n=2}^{N}\sum_{m=1}^{M}[\lambda(a_{n,m}c^{\dagger}_{n-1,m}+b_{n,m}d^{\dagger}_{n-1,m})] \\ & +\sum_{n=1}^{N}\sum_{m=2}^{M}[\lambda(a_{n,m}b^{\dagger}_{n,m-1}+c_{n,m}d^{\dagger}_{n,m-1})]+\text{H.c.}, \end{aligned} \quad (1)$$

where $q^{\dagger}_{n,m}$ ($q_{n,m}$) with $q = \{a, b, c, d\}$ representing the creation (annihilation) operator for the photonic mode (A–D) at lattice site (n, m). To detect the robustness of the system, in the numerical calculations, we will consider the disorder effect of the parameters with $\omega + \epsilon$, $\gamma + \epsilon$, $\lambda + \epsilon$, and $J + \epsilon$, where $\epsilon \in [-\lambda/100, \lambda/100]$ is randomly distributed.

The 2D SSH model can be implemented in a network of coupled superconducting transmission line resonators [74–76]

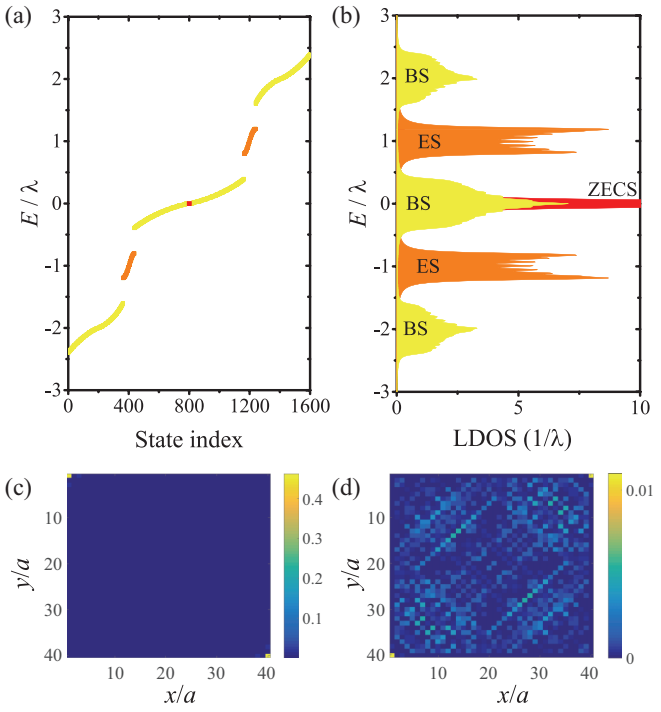

FIG. 2. (a) Energy spectrum for a 2D SSH model with a 20×20 array of unit cells with $\gamma = \lambda/5$ and $J = 0$. The orange (gray) bands denote the the topological ESs of the lattice, the bulk states (BSs) are depicted by yellow (light gray) bands and the four degenerate zero-energy corner states (ZECSs) appear at zero energy with a red (dark gray) point. (b) The local density of states (LDOS) with where the ZECS for mode A at lattice site (1,1), the ES for mode A at lattice site (1,11), and the BS for mode A at lattice site (11,11). The field profiles of the corner states without disorder in (c) and with disorder $\epsilon \in [-\lambda/100, \lambda/100]$ in (d).

as schematically shown in Fig. 1(b). Resonators B and C are connected by an auxiliary capacitor (in red) as shown in Fig. 1(c). The 2D SSH model can also be realized using a 2D lattice of nanophotonic silicon ring resonators as reported in Ref. [66]. These ring B's and ring C's can be coupled to each other using an auxiliary ring (in red) as shown in Fig. 1(d).

III. GENERAL BOUNDED CORNER STATES

First of all, let us review the corner state in the 2D SSH model without intracellular NNN hopping, i.e., $J = 0$. The energy spectrum for a 2D SSH model without intracellular NNN hopping is shown in Fig. 2(a). There are five bands, two orange (gray) are edge-state bands and three yellow (light gray) are bulk-state bands. The energy bands can be reflected in the LDOS as shown in Fig. 2(b). The LDOS can be calculation based on the Green's function in frequency space (see Ref. [77] or the Appendix), and the photonic LDOS is experimentally accessible via reflection/transmission measurements.

Figure 2(c) shows that the 2D SSH model with zero gauge flux hosts zero-energy states localized at the corners, similar to those of the 2D SSH model with π gauge flux [62–64,66]. However, there is no band gap at zero energy in the energy spectrum of the model as shown in Fig. 2(b), which indicates

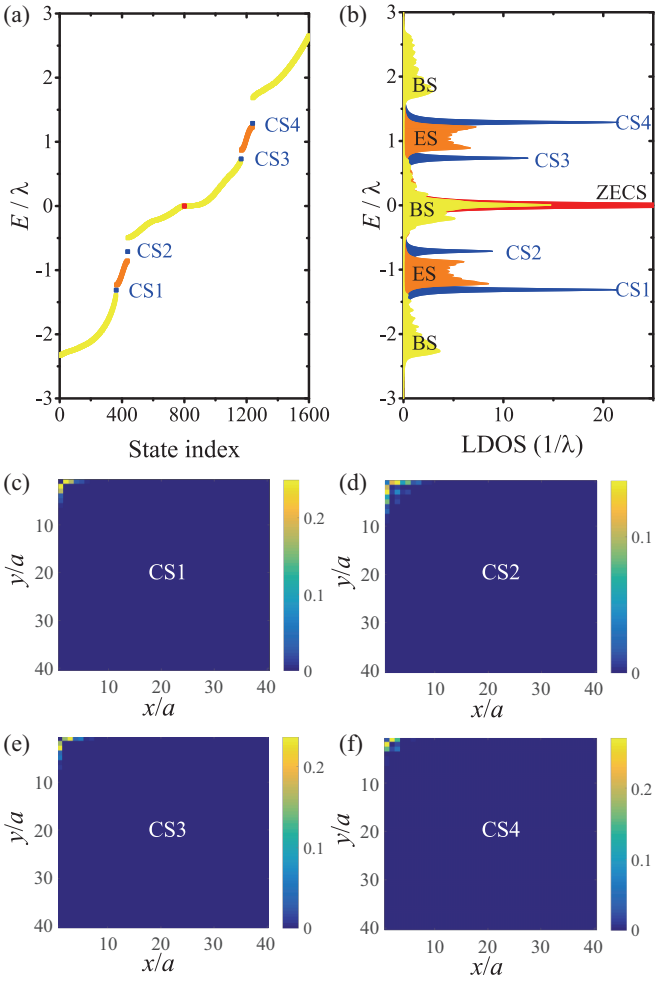

FIG. 3. (a) Energy spectrum for a 2D SSH model with a 20×20 array of unit cells with $\gamma = \lambda/5$ and $J = \lambda/2$. (b) Corresponding LDOS with $\kappa = \lambda/20$. The general bounded corner states [CS1–CS4, LDOS for mode B at lattice site (1,1)] appear in the band gaps between the edge and bulk bands. The field profiles of the general bounded corner states CS1–CS4 in (c)–(f) with disorder $\epsilon \in [-\lambda/100, \lambda/100]$.

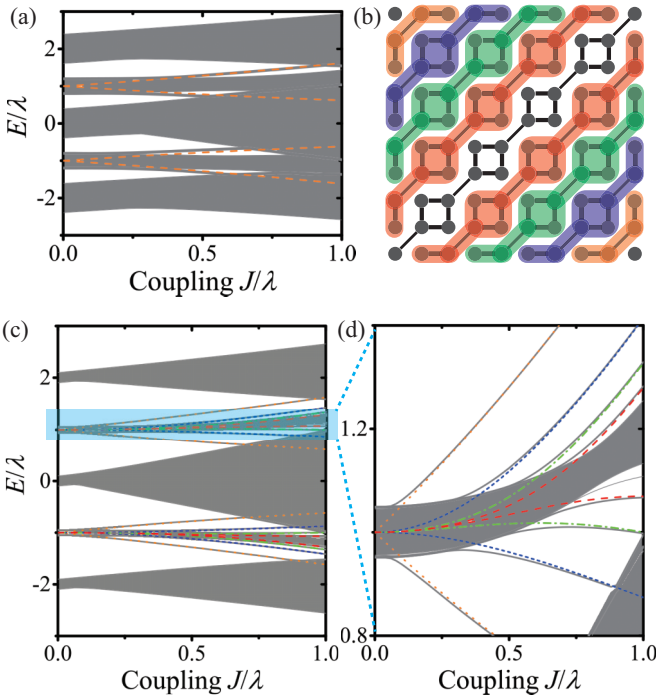

FIG. 4. (a) Energy spectrum of a 2D SSH model with varying intercellular NNN hopping J/λ with $\gamma = \lambda/5$. (b) Illustration of coupling between modes around the corners forming general bounded corner states with $\gamma = 0$. (c) Energy spectrum of a 2D SSH model with varying intercellular NNN hopping J/λ with $\gamma = \lambda/20$. (d) Enlarged section of (c) showing the emergence of more corner states from the bands of edge states as J increases where the colored (dotted orange, short dashed blue, dash-dotted green, and dashed red) curves show the analytical result for the energies of corner states obtained with modes around the corners highlighted in the same color in (b).

that this zero-energy corner states are not topologically protected and are susceptible to the fabrication disorders. Consequently, the disorder, which is a very common phenomenon in the experimental setups, can easily couple these corner states to the bulk states located near zero energy as shown in the field profiles of the zero-energy corner states with disorder $\epsilon \in [-\lambda/100, \lambda/100]$ in Fig. 2(d). These agree with a recently experimental result [66]. As this type of zero-energy corner state is susceptible to the fabrication disorders and appears even in the absence of intracellular NNN hoppings, we will not explore it in the following.

Next, we demonstrate that new corner states can be induced by the intracellular NNN hopping, even if there is no gauge flux through the lattice of the 2D SSH model. As shown in the energy spectrum [Fig. 3(a)] and LDOS [Fig. 3(b)], besides the corner states at zero energy (in red), there are four double degenerate corner states CS1–CS4 (highlighted in blue or dark gray) that appear in the band gaps between the edge and the bulk bands. Similar corner states have been observed in a 2D topological photonic crystal with a kagome lattice very recently [73].

Here, we analyze the characteristics of the new corner states with the field profiles shown in Figs. 3(c)–3(f). (i) Different from the conventional corner states observed before, the new corner states are localized around the corners but not at the four corner points $(x/a, y/a) = \{(1, 1), (1, 2M), (2N, 1), (2N, 2M)\}$. The highest values of the field profiles appear around the points $(x/a, y/a) = \{(1, 2), (1, 3), (2, 1), (3, 1)\}$ or $(x/a, y/a) = \{(2N-1, 2M), (2N-2, 2M), (2N, 2M-1), (2N, 2M-2)\}$ (not shown in the figures). Physically, the conventional corner states appear in the HOTIs, but the new corner states are the stable bounded states split off from the edge-state bands by the intracellular NNN hoppings (we will show later on). Thus, we refer to these new corner states as general bounded corner states. (ii) The field profiles show that the general bounded corner states are robust to random noises. This point is also evident in the energy spectrum and LDOS of the system where the general bounded corner states are separated from the edge and bulk bands [Figs. 3(a) and 3(b)].

To reveal the origin of general bounded corner states, the energy spectrum of a 2D SSH model are plotted with varying intracellular NNN hopping J/λ in Fig. 4(a). It is obvious that,

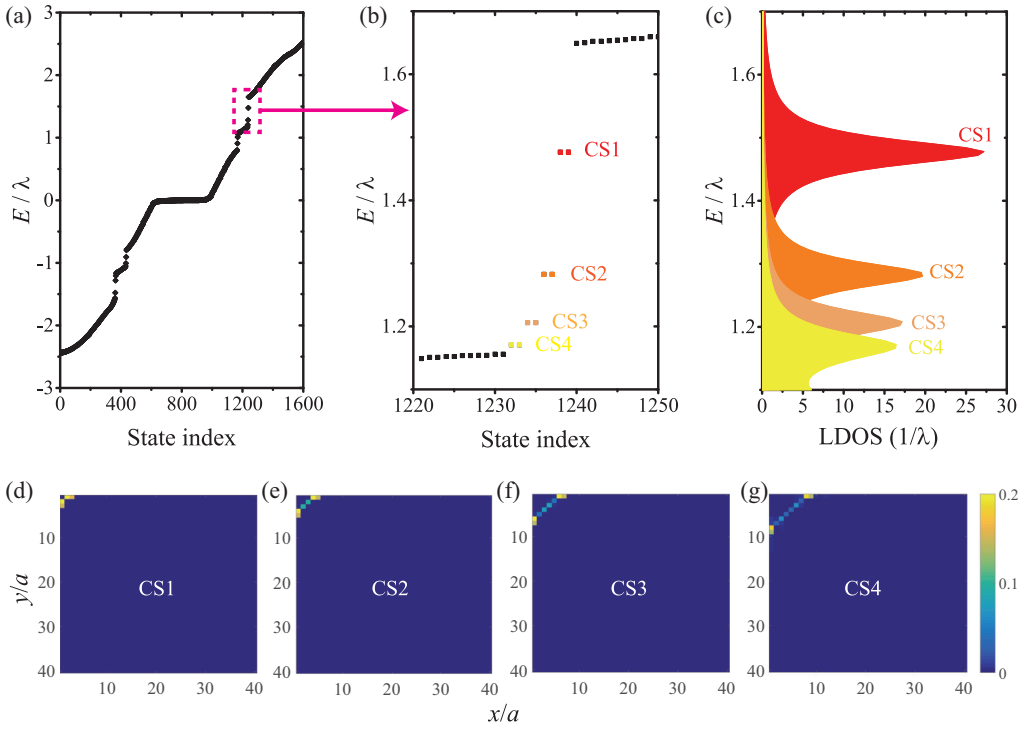

FIG. 5. (a) Energy spectrum for a 2D SSH model with a 20×20 array of unit cells with $\gamma = \lambda/20$ and $J = 0.8\lambda$. (b) Enlarged section of (a) showing four general bounded corner states: CS1–CS4. (c) LDOS of the general bounded corner states CS1–CS4 with $\kappa = \lambda/20$ for mode B at lattice sites (1,1), (2,2), (3,3), and (4,4) respectively. (d)–(g) Corresponding field profiles of the corner states CS1–CS4 with disorder $\epsilon \in [-\lambda/100, \lambda/100]$.

the general bounded corner states split off from the edge-state bands with the increasing of J/λ. The general bounded corner states can be understood from the model in the case of $\gamma = 0$ as shown in Fig. 4(b) where the 2D SSH model has been divided into separate model fragments highlighted in different colors. The dashed orange lines in Fig. 4(a) show the analytical result for the energies of corner states obtained with modes around the corners highlighted in orange, which agree with the energy spectrum of general bounded corner states, and the subtle differences are induced by the intracellular hopping γ.

To show the general bounded corner states induced by the other separate model fragments in different colors, the energy spectrum of a 2D SSH model with $\gamma = \lambda/20$ is plotted as a function of J/λ in Figs. 4(c) and 4(d). Interestingly, more general bounded corner states split off from the edge-state bands with the increasing of the intracellular NNN hopping J/λ. The energy of the general corner states agree well with analytical results (dotted orange, short dashed blue, dash-dotted green, and dashed red curves) obtained with modes around the corners highlighted in the same color in Fig. 4(b).

To further explore the characteristics of the general bounded corner states, the energy spectrum for a 2D SSH model are shown in Figs. 5(a) and 5(b) with $\gamma = \lambda/20$ and $J = 0.8\lambda$. There are four double degenerate corner states CS1–CS4 that appear in the band gap between the edge and the bulk bands. These general bounded corner states can be observed by the LDOS of the system as shown in Fig. 5(c). The corresponding field profiles of the general bounded corner states are shown in Figs. 5(d)–5(g), which agree well with the separate model fragments in Fig. 4(b).

IV. CONCLUSIONS

In conclusion, we have demonstrated that the 2D SSH model on a square lattice without gauge flux can support robust general bounded corner states by considering the intracellular NNN hoppings. We have analytically determined that the intracellular NNN hoppings can result in the formation of a broad class of general bounded corner states, which can be understood intuitively by the separate model fragments of the 2D SSH model. We believe that our paper opens important directions in inducing unique corner states by the intracellular NNN hoppings (long-range interactions) and offering possibilities to control photons in novel ways.

ACKNOWLEDGMENTS

X.-W.X. was supported by the Key Program of Natural Science Foundation of Jiangxi Province, China under Grant No. 20192ACB21002 and the National Natural Science Foundation of China (NSFC) under Grant No. 11604096. Z.-F.L. was supported by the NSFC under Grant No. 11864012. A.-X.C. was supported by the NSFC under Grant No. 11775190.

APPENDIX: CALCULATION OF THE LDOS

Substituting the Hamiltonian (1) into the Heisenberg equation and taking into account the damping of the modes with

damping rate κ and the corresponding quantum noises, we get the quantum Langevin equations (QLEs) for the operators in the unit cell with cell index (n, m) as

$$i\frac{d}{dt}a_{n,m} = -i\frac{\kappa}{2}a_{n,m} + \gamma(b_{n,m} + c_{n,m}) + \lambda(b_{n,m-1} + c_{n-1,m}) + i\sqrt{\kappa}a^{(\mathrm{in})}_{n,m}, \tag{A1}$$

$$i\frac{d}{dt}b_{n,m} = -i\frac{\kappa}{2}b_{n,m} + \gamma(a_{n,m} + d_{n,m}) + \lambda(a_{n,m+1} + d_{n-1,m}) + Jc_{n,m} + i\sqrt{\kappa}b^{(\mathrm{in})}_{n,m}, \tag{A2}$$

$$i\frac{d}{dt}c_{n,m} = -i\frac{\kappa}{2}c_{n,m} + \gamma(a_{n,m} + d_{n,m}) + \lambda(a_{n+1,m} + d_{n,m-1}) + Jb_{n,m} + i\sqrt{\kappa}c^{(\mathrm{in})}_{n,m}, \tag{A3}$$

$$i\frac{d}{dt}d_{n,m} = -i\frac{\kappa}{2}d_{n,m} + \gamma(b_{n,m} + c_{n,m}) + \lambda(b_{n+1,m} + c_{n,m+1}) + i\sqrt{\kappa}d^{(\mathrm{in})}_{n,m}, \tag{A4}$$

where $q^{(\mathrm{in})}_{n,m}$ $(q = a, b, c, d)$ is the input quantum noise operators.

In order to calculate LDOS numerically in a finite system with $N\times M$ unit cells, the QLEs can be concisely expressed as

$$i\frac{dC}{dt} = AC + i\sqrt{\kappa}C_{\mathrm{in}}, \tag{A5}$$

where $C = (\ldots, a_l, b_l, c_l, d_l, \ldots)^T$ and $C_{\mathrm{in}} = (\ldots, a^{(\mathrm{in})}_l, b^{(\mathrm{in})}_l, c^{(\mathrm{in})}_l, d^{(\mathrm{in})}_l, \ldots)^T$ are $4NM$-dimensional vectors with the cell index $l = (n, m)$, and A is the $4NM\times 4NM$ coefficient matrix. The Green's function for photons with relative energy E is given by

$$G = \frac{1}{E - A}. \tag{A6}$$

The LDOS is determined by

$$\rho(E, l_q) = -2\,\mathrm{Im}\,G(E, l_q, l_q), \tag{A7}$$

with subscript $q = a, b, c, d$.

[1] T. Ozawa, H. M. Price, A. Amo, N. Goldman, M. Hafezi, L. Lu, M. C. Rechtsman, D. Schuster, J. Simon, O. Zilberberg, and I. Carusotto, Rev. Mod. Phys. **91**, 015006 (2019).

[2] B. Bahari, A. Ndao, F. Vallini, A. El Amili, Y. Fainman, and B. Kanté, Science **358**, 636 (2017).

[3] G. Harari, M. A. Bandres, Y. Lumer, M. C. Rechtsman, Y. D. Chong, M. Khajavikhan, D. N. Christodoulides, and M. Segev, Science **359**, eaar4003 (2018).

[4] M. A. Bandres, S. Wittek, G. Harari, M. Parto, J. Ren, M. Segev, D. N. Christodoulides, and M. Khajavikhan, Science **359**, eaar4005 (2018).

[5] Y. Zeng, U. Chattopadhyay, B. Zhu, B. Qiang, J. Li, Y. Jin, L. Li, A. G. Davies, E. H. Linfield, B. Zhang, Y. Chong, and Q. J. Wang, Nature (London) **578**, 246 (2020).

[6] W. Zhang, X. Xie, H. Hao, J. Dang, S. Xiao, S. Shi, H. Ni, Z. Niu, C. Wang, K. Jin, X. Zhang, and X. Xu, arXiv:2002.06513.

[7] B. Zhen, C. W. Hsu, Y. Igarashi, L. Lu, I. Kaminer, A. Pick, S.-L. Chua, J. D. Joannopoulos, and M. Soljačić, Nature (London) **525**, 354 (2015).

[8] H. Zhao, X. Qiao, T. Wu, B. Midya, S. Longhi, and L. Feng, Science **365**, 1163 (2019).

[9] S. Malzard, C. Poli, and H. Schomerus, Phys. Rev. Lett. **115**, 200402 (2015).

[10] S. Weimann, M. Kremer, Y. Plotnik, Y. Lumer, S. Nolte, K. Makris, M. Segev, M. C. Rechtsman, and A. Szameit, Nat. Mater. **16**, 433 (2016).

[11] T. E. Lee, Phys. Rev. Lett. **116**, 133903 (2016).

[12] Y. Xu, S.-T. Wang, and L.-M. Duan, Phys. Rev. Lett. **118**, 045701 (2017).

[13] F. K. Kunst, E. Edvardsson, J. C. Budich, and E. J. Bergholtz, Phys. Rev. Lett. **121**, 026808 (2018).

[14] S. Yao and Z. Wang, Phys. Rev. Lett. **121**, 086803 (2018).

[15] H. Shen, B. Zhen, and L. Fu, Phys. Rev. Lett. **120**, 146402 (2018).

[16] Z. Gong, Y. Ashida, K. Kawabata, K. Takasan, S. Higashikawa, and M. Ueda, Phys. Rev. X **8**, 031079 (2018).

[17] T. Liu, Y.-R. Zhang, Q. Ai, Z. Gong, K. Kawabata, M. Ueda, and F. Nori, Phys. Rev. Lett. **122**, 076801 (2019).

[18] C. H. Lee, L. Li, and J. Gong, Phys. Rev. Lett. **123**, 016805 (2019).

[19] C. Yin, H. Jiang, L. Li, R. Lü, and S. Chen, Phys. Rev. A **97**, 052115 (2018).

[20] W. Hu, H. Wang, P. P. Shum, and Y. D. Chong, Phys. Rev. B **95**, 184306 (2017).

[21] K. Kawabata, K. Shiozaki, and M. Ueda, Phys. Rev. B **98**, 165148 (2018).

[22] V. M. Martinez Alvarez, J. E. Barrios Vargas, and L. E. F. Foa Torres, Phys. Rev. B **97**, 121401(R) (2018).

[23] L. Jin and Z. Song, Phys. Rev. B **99**, 081103(R) (2019).

[24] C. H. Lee and R. Thomale, Phys. Rev. B **99**, 201103(R) (2019).

[25] D. S. Borgnia, A. J. Kruchkov, and R.-J. Slager, Phys. Rev. Lett. **124**, 056802 (2020).

[26] J. Koch, A. A. Houck, K. L. Hur, and S. M. Girvin, Phys. Rev. A **82**, 043811 (2010).

[27] Y. Lumer, Y. Plotnik, M. C. Rechtsman, and M. Segev, Phys. Rev. Lett. **111**, 243905 (2013).

[28] P. Roushan, C. Neill, A. Megrant, Y. Chen, R. Babbush, R. Barends, B. Campbell, Z. Chen, B. Chiaro, A. Dunsworth, A. Fowler, E. Jeffrey, J. Kelly, E. Lucero, J. Mutus, P. J. J. O'Malley, M. Neeley, C. Quintana, D. Sank, A. Vainsencher, J. Wenner, T. White, E. Kapit, H. Neven, and J. Martinis, Nat. Phys. **13**, 146 (2016).

[29] D. Leykam and Y. D. Chong, Phys. Rev. Lett. **117**, 143901 (2016).

[30] Y. Hadad, A. B. Khanikaev, and A. Alù, Phys. Rev. B **93**, 155112 (2016).

[31] X. Zhou, Y. Wang, D. Leykam, and Y. D. Chong, New J. Phys. **19**, 095002 (2017).

[32] R. Chaunsali and G. Theocharis, Phys. Rev. B **100**, 014302 (2019).

[33] X.-W. Luo, X. Zhou, C.-F. Li, J.-S. Xu, G.-C. Guo, and Z.-W. Zhou, Nat. Commun. **6**, 7704 (2015).

[34] X.-F. Zhou, X.-W. Luo, S. Wang, G.-C. Guo, X. Zhou, H. Pu, and Z.-W. Zhou, Phys. Rev. Lett. **118**, 083603 (2017).

[35] L. Yuan, Q. Lin, M. Xiao, and S. Fan, Optica **5**, 1396 (2018).

[36] T. Ozawa and H. M. Price, Nat. Rev. Phys. **1**, 349 (2019).

[37] E. Lustig, S. Weimann, Y. Plotnik, Y. Lumer, M. Bandres, A. Szameit, and M. Segev, Nature (London) **567**, 356 (2019).

[38] A. Dutt, M. Minkov, and S. Fan, arXiv:1911.11310.

[39] A. Dutt, Q. Lin, L. Yuan, M. Minkov, M. Xiao, and S. Fan, Science **367**, 59 (2020).

[40] W. Zhang and X. Zhang, arXiv:1906.02967.

[41] W. A. Benalcazar, B. A. Bernevig, and T. L. Hughes, Science **357**, 61 (2017).

[42] J. Langbehn, Y. Peng, L. Trifunovic, F. von Oppen, and P. W. Brouwer, Phys. Rev. Lett. **119**, 246401 (2017).

[43] Z. Song, Z. Fang, and C. Fang, Phys. Rev. Lett. **119**, 246402 (2017).

[44] W. A. Benalcazar, B. A. Bernevig, and T. L. Hughes, Phys. Rev. B **96**, 245115 (2017).

[45] F. Schindler, A. M. Cook, M. G. Vergniory, Z. Wang, S. S. P. Parkin, B. A. Bernevig, and T. Neupert, Sci. Adv. **4**, eaat0346 (2018).

[46] Q.-B. Zeng, Y.-B. Yang, and Y. Xu, Phys. Rev. B **101**, 241104(R) (2020).

[47] Y.-B. Yang, K. Li, L.-M. Duan, and Y. Xu, arXiv:1910.04151.

[48] M. Ezawa, Phys. Rev. Lett. **120**, 026801 (2018).

[49] X. Zhu, Phys. Rev. B **97**, 205134 (2018).

[50] M. Geier, L. Trifunovic, M. Hoskam, and P. W. Brouwer, Phys. Rev. B **97**, 205135 (2018).

[51] E. Khalaf, Phys. Rev. B **97**, 205136 (2018).

[52] F. Schindler, Z. Wang, M. Vergniory, A. Cook, A. Murani, S. Sengupta, A. Kasumov, R. Deblock, S. Jeon, I. Drozdov, H. Bouchiat, S. Guéron, A. Yazdani, B. Bernevig, and T. Neupert, Nat. Phys. **14**, 918 (2018).

[53] J. Bao, D. Zou, W. Zhang, W. He, H. Sun, and X. Zhang, Phys. Rev. B **100**, 201406(R) (2019).

[54] R.-J. Slager, L. Rademaker, J. Zaanen, and L. Balents, Phys. Rev. B **92**, 085126 (2015).

[55] J. Noh, W. A. Benalcazar, S. Huang, M. J. Collins, K. P. Chen, T. L. Hughes, and M. C. Rechtsman, Nat. Photon. **12**, 408 (2018).

[56] F. Zangeneh-Nejad and R. Fleury, Phys. Rev. Lett. **123**, 053902 (2019).

[57] H. Fan, B. Xia, L. Tong, S. Zheng, and D. Yu, Phys. Rev. Lett. **122**, 204301 (2019).

[58] H. Xue, Y. Yang, F. Gao, Y. Chong, and B. Zhang, Nat. Mater. **18**, 108 (2018).

[59] X. Ni, M. Weiner, A. Alù, and A. Khanikaev, Nat. Mater. **18**, 113 (2019).

[60] A. Hassan, F. Kunst, A. Moritz, G. Andler, E. Bergholtz, and M. Bourennane, Nat. Photon. **13**, 697 (2019).

[61] Y. Chen, X. Lu, and H. Chen, Opt. Lett. **44**, 4251 (2019).

[62] M. Serra-Garcia, V. Peri, R. Süsstrunk, O. R. Bilal, T. Larsen, L. G. Villanueva, and S. D. Huber, Nature (London) **555**, 342 (2018).

[63] C. W. Peterson, W. A. Benalcazar, T. L. Hughes, and G. Bahl, Nature (London) **555**, 346 (2018).

[64] S. Imhof, C. Berger, F. Bayer, J. Brehm, L. W. Molenkamp, T. Kiessling, F. Schindler, C. H. Lee, M. Greiter, T. Neupert, and R. Thomale, Nat. Phys. **14**, 925 (2018).

[65] M. Serra-Garcia, R. Süsstrunk, and S. D. Huber, Phys. Rev. B **99**, 020304(R) (2019).

[66] S. Mittal, V. V. Orre, G. Zhu, M. A. Gorlach, A. Poddubny, and M. Hafezi, Nat. Photon. **13**, 692 (2019).

[67] X.-D. Chen, W.-M. Deng, F.-L. Shi, F.-L. Zhao, M. Chen, and J.-W. Dong, Phys. Rev. Lett. **122**, 233902 (2019).

[68] B.-Y. Xie, G.-X. Su, H.-F. Wang, H. Su, X.-P. Shen, P. Zhan, M.-H. Lu, Z.-L. Wang, and Y.-F. Chen, Phys. Rev. Lett. **122**, 233903 (2019).

[69] Y. Ota, F. Liu, R. Katsumi, K. Watanabe, K. Wakabayashi, Y. Arakawa, and S. Iwamoto, Optica **6**, 786 (2019).

[70] X. Zhang, H.-X. Wang, Z.-K. Lin, Y. Tian, B. Xie, M.-H. Lu, Y.-F. Chen, and J.-H. Jiang, Nat. Phys. **15**, 582 (2019).

[71] D. Leykam, S. Mittal, M. Hafezi, and Y. D. Chong, Phys. Rev. Lett. **121**, 023901 (2018).

[72] C. Poli, H. Schomerus, M. Bellec, U. Kuhl, and F. Mortessagne, 2D Mater. **4**, 025008 (2017).

[73] M. Li, D. Zhirihin, M. Gorlach, X. Ni, D. Filonov, A. Slobozhanyuk, A. Alù, and A. Khanikaev, Nat. Photon. **14**, 89 (2020).

[74] D. M. Pozar, *Microwave Engineering*, 4th ed. (John Wiley and Sons, Inc., New York, 2011).

[75] A. Wallraff, D. I. Schuster, A. Blais, L. Frunzio, R.-S. Huang, J. Majer, S. Kumar, S. M. Girvin, and R. J. Schoelkopf, Nature (London) **431**, 162 (2004).

[76] X. Gu, A. F. Kockum, A. Miranowicz, Y. X. Liu, and F. Nori, Phys. Rep. **718–719**, 1 (2017).

[77] V. Peano, C. Brendel, M. Schmidt, and F. Marquardt, Phys. Rev. X **5**, 031011 (2015).